ADVANCED FUNCTIONAL MATERIALS
www.afm-journal.de

Programmable Biopolymers for Advancing Biomedical Applications of Fluorescent Nanodiamonds

Yuzhou Wu, Anna Ermakova, Weina Liu, Goutam Pramanik, Tran Minh Vu, Andrea Kurz, Liam McGuinness, Boris Naydenov, Susanne Hafner, Rolf Reuter, Joerg Wrachtrup, Junichi Isoya, Christina Förtsch, Holger Barth, Thomas Simmet, Fedor Jelezko,* and Tanja Weil**

A versatile biopolymer platform for advancing nanodiamonds (NDs) as unique magnetooptic materials for biomedical applications is presented here. Precision biopolymer coatings are designed by chemical reprogramming the functionalities of serum albumin via a straightforward synthesis protocol. Such biopolymers offer high biocompatibility and precise modification with various functional entities due to the large number of available reactive amino acid residues. Premodification of these biopolymers provides a convenient approach to customized surface functionalization of NDs. As an example, the anticancer drug doxorubicin (DOX) is conjugated to the biopolymer with high reproducibility and full characterization. The biopolymer-coated NDs reveal excellent colloidal stabilities in all physiological media tested, even after loading with high numbers of hydrophobic DOX. The intracellular distribution of NDs and DOX is analyzed in living cells by recording the fluorescence spectra in different cellular compartments, which proves efficient intracellular release of DOX from the carrier. Studies in vitro as well as in a chick tumor xenograft model reveal efficient antitumor effects. The facile and versatile biopolymer coating strategy reported herein will greatly accelerate the availability of customized NDs with reliable and reproducible features to exploit their great potential in single molecular bioimaging, in vivo biosensing, and high resolution quantum optics.

1. Introduction

Since the past decade, fluorescent nanodiamonds (FNDs) are emerging as highly promising nanoparticles for biomedical applications due to their unique optical and magnetic properties.[1] FNDs are obtained by implementing elemental defects into the carbon lattice, e.g., nitrogen vacancy (N-V), giving unconditionally stable fluorescence without bleaching or blinking even after several months of continuous excitation.[2] The emission wavelength of FNDs is not size dependent and is tunable from the visible to the near infrared region according to the elemental defects.[3] In addition, the N-V center in FNDs serves as single-spin sensor that locally detects many valuable physical properties, such as temperature, magnetic fields and electric resonance in a biological microenvironment.[4]

Unlike many other metal or semiconductor nanoparticles, nanodiamonds (NDs) are considered chemically inert

Dr. Y. Wu, W. Liu, Dr. G. Pramanik, Prof. T. Weil
Department of Organic Chemistry III/Macromolecular Chemistry
Ulm University
Albert-Einstein-Allee 11, 89081 Ulm, Germany
E-mail: yuzhou.wu@uni-ulm.de; tanja.weil@uni-ulm.de
A. Ermakova, T. M. Vu, A. Kurz, L. McGuinness, Dr. B. Naydenov, Prof. F. Jelezko
Institut für Quantenoptik
Ulm University
Albert-Einstein-Allee 11, 89081 Ulm, Germany
E-mail: fedor.jelezko@uni-ulm.de
Dr. S. Hafner, Prof. T. Simmet
Institute of Pharmacology of Natural Products and Clinical Pharmacology
Ulm University
Helmholtzstr. 20, 89081 Ulm, Germany
Dr. R. Reuter, Prof. J. Wrachtrup
Physikalisches Institut
University of Stuttgart
70569 Stuttgart, Germany
Prof. J. Isoya
Research Center for Knowledge Communities
University of Tsukuba
1-2 Kasuga, Tsukuba, Ibaraki 305-8550, Japan
Dr. C. Förtsch, Prof. H. Barth
Institute of Pharmacology and Toxicology
University of Ulm Medical Center
Albert-Einstein-Allee 11, 89081 Ulm, Germany

DOI: 10.1002/adfm.201502704

in living systems with minimal toxicity risk.[5] Based on the in vitro and in vivo studies reported until now, NDs are among the most biocompatible nanoparticles with promising biosafety profile.[6] Therefore, they are very promising sensor probes for developing the next generation biosensing in vivo, as well as attractive nanomedicine platforms for delivery of chemotherapeutics,[7] proteins,[8] and genes.[9] Different formulations of ND-based drug delivery systems has been reported including physical absorption of lipophilic drug molecules into detonation ND clusters[10] and chemical modification of drug molecules onto ND surface.[11] Promising progress has been made to address targeted drug delivery, controlled drug release, intracellular tracking and evading chemoresistance in vitro and in vivo.[7d,e,11b,12] Some preclinical studies have shown that ND formulation could significantly increase the drug efficacy to drug resistant liver and breast cancer in murine model[10b,12b] by increasing drug retention in tumor tissue, minimizing liver toxicity and systemic toxicity, and expending the therapeutic window.[10b,12b] All these studies showed the promising translational potential of NDs as drug delivery carriers. In addition, due to the unique opportunities to combine fluorescence or magnetic resonance based imaging together with therapeutic properties within one particle,[13] FNDs offer great promise as a platform for evolving new concepts of "theranostics" (a portmanteau of therapeutics and diagnostics).[14]

Although FNDs offer many intriguing opportunities for biomedical applications, their extensive use in a biological environment is still limited by two major challenges: 1) their strong aggregation in biological systems and 2) their challenging surface chemistry. Several methods have been reported to functionalize the ND surface directly by chemical reactions[15] and all have their merits and limitations. Previously, encapsulation within a biocompatible shell has been proposed as an effective strategy for the reproducible biofunctionalization of NDs. Polymeric and inorganic shells (e.g., silica) have been introduced to increase the colloidal stability and facilitate surface functionalization after coating.[16] Nevertheless, traceable and reproducible ND surface chemistry and high colloidal stability under physiological conditions even after loading high amount of drug molecules remain a major concerns (Table S2, Supporting Information). To address these challenges, the synthesis of biocompatible, well-defined polymers, and their functionalization before coating might offer a worthy alternative to customize NDs with precisely defined surface groups.

Herein, we propose a multifunctional biopolymer platform based on the abundant blood plasma protein human serum albumin (HSA) that is converted into a multivalent, biocompatible and programmable precision biopolymer[17] that efficiently encapsulates FNDs and imparts versatile and reproducible surface functionalization. NDs functionalized by this approach offer excellent colloidal stability in all tested physiologically relevant buffers and media, even at very high salt concentrations and facilitate anticancer drug delivery with controlled drug release and efficient antitumor activity.

As strength, all precision biopolymers are fully characterized before coating thus ensuring the presence of all essential ND surface functions. This compares favorably to a direct modification of the ND surface, which makes it difficult to control the presence of all desired surface groups. Our novel coating strategy benefits from the nontoxic and biocompatible nature of the HSA polypeptide backbone, which is simultaneously serving as a versatile and reproducible platform to achieve highly stable and multifunctional FNDs for various biomedical applications.

2. Results and Discussion

2.1. Preparation and Characterization of Multifunctional NDs/FNDs

2.1.1. Preparation and Characterization of the NDs/FNDs

All NDs used in this study were obtained by milling of high-pressure high-temperature synthesized diamond crystals (Ib). These NDs already contained substitutional nitrogen atoms during crystal growth. Irradiation with high energy electrons and subsequent annealing resulted in high concentrations of N-V centers (more than 90% of FNDs contain N-V centers, see Figure S2, Supporting Information) that offer stable and non-bleaching fluorescence. N-V centers in these NDs are significantly more stable in comparison to N-V centers in detonation NDs that are often used in other studies.[18] The NDs were further oxidized with strong acids to remove amorphous carbon on diamond crystals and convert the surface sp^2 carbon to carboxyl groups yielding highly negatively charged surfaces (zeta potential = −44 ± 0.8 mV). The resulting NDs are soluble in water with an average hydrodynamic diameter of 47.4 ± 0.2 nm (polydispersity index (PDI) = 0.17) according to dynamic light scattering (DLS). However, they formed larger aggregates under physiological conditions as reported previously.[19]

2.1.2. Preparation of the Biopolymer Coatings as Versatile ND/FND Functionalization Platform

HSA precision biopolymers were obtained by unfolding the polypeptide backbone of native HSA in urea and in situ stabilizing the unfolded polypeptide with polyethylene glycol (PEG) chains.[17] Similar to synthetic polymers, protein-derived biopolymers provide high molecular weights to efficiently coat and passivate the ND surface. Their high structural definition with precisely defined monomer sequences and contour lengths provides unique avenues for attaching distinct numbers of functional groups at predefined locations along the polypeptide backbone.[20] Positively charged HSA biopolymer **1** (dcHSA-PEG, **Figure 1**) was prepared that forms very stable polyplexes with NDs. First, native HSA was converted into cationic HSA (cHSA) containing ≈158 positively charged primary amino groups[21] (see detailed calculation in the Supporting Information and Figure S4, Supporting Information). Thereafter, on average 16 PEG chains (M_w = 2000) were conjugated to the amino groups of cHSA to afford cHSA-PEG$(2000)_{16}$ (Figure S5, Supporting Information). Introducing PEG(2000) chains is essential to impart high colloidal stability in aqueous media and to reduce plasma protein binding, due to the extended hydration shell provided by

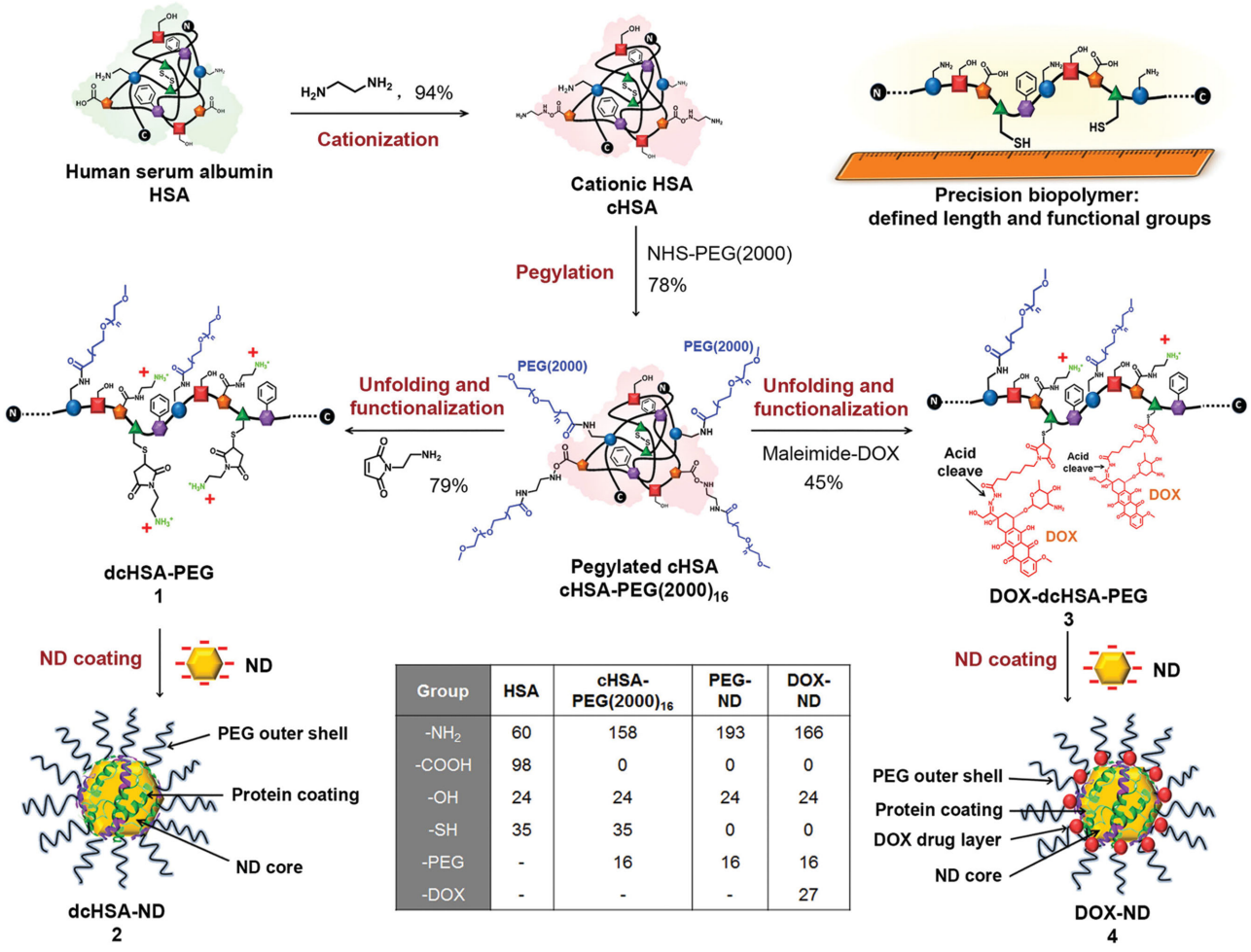

Group	HSA	cHSA-PEG(2000)$_{16}$	PEG-ND	DOX-ND
-NH_2	60	158	193	166
-COOH	98	0	0	0
-OH	24	24	24	24
-SH	35	35	0	0
-PEG	-	16	16	16
-DOX	-	-	-	27

Figure 1. Preparation of dcHSA-ND and DOX-ND.

the PEG chains.[22] cHSA-PEG(2000)$_{16}$ was denatured in concentrated urea buffer, followed by reduction of the disulfide bridges by the mild reduction agent tris(2-carboxyethyl)phosphine (TCEP) and capping of the free sulfurhydryl groups with *N*-(2-aminoethyl)maleimide to obtain the stable single chain biopolymer dcHSA-PEG **1** (Figure S1, Supporting Information). This biopolymer (**1**) is highly positively charged (zeta potential of **1** = 13.6 ± 0.8 mV), providing multiple electrostatic interactions with the negatively charged ND surface as well as hydrophobic amino acids of HSA that could also contribute to an improved stabilization of the NDs by interacting with nonpolar ND surface areas.

dcHSA-PEG (**1**) represents a versatile platform for imparting desired functionalities to the ND surface, due to the large and well-defined number of functional groups of the amino acid side chains (see the insert table in Figure 1 and details in Figure S4, Supporting Information). Since ND-based drug delivery systems are of emerging interest as theranostics,[11] we have challenged our biopolymer platform by introducing the anticancer agent doxorubicin (DOX). DOX is an important chemotherapeutic drug that displays cytotoxicity in cancer but possibly also in healthy cells. Specifically, induction of cardiac toxicity may lead to severe adverse effects, which severely limit the therapeutic efficacy of DOX.[23] Therefore, DOX is a prime candidate for nanoparticle-boosted drug delivery, which requires the attachment of reproducible DOX amounts as well as efficient release from the NDs. Achieving high colloidal stability even after loading high numbers of such drug molecules still remains a major challenge since the attachment of polyaromatic compounds onto the nanoparticle surface considerably increases the formation of ND aggregates (Table S2, Supporting Information).[18a]

DOX was conjugated onto biopolymer (**1**) by using the DOX prodrug *N*-ε-maleimidocaproic acid hydrazide-DOX (EMCH-DOX), which contains a maleimide group reacting with the cysteine residues on HSA and an acid cleavable hydrazone linker allowing DOX release inside acidic cell compartments. According to the amino acid sequence of HSA, 35 cysteines are available, eight of which are in direct vicinity (Figure S4, Supporting Information). In consequence, 27 EMCH-DOX could be conjugated onto the dcHSA-PEG (**1**) in a highly reproducible fashion yielding DOX-loaded biopolymer (**3**). The number of DOX on biopolymer (**3**) has been confirmed by both DOX absorbance and matrix-assisted laser desorption ionization (MALDI) mass spectrometry (Figure S8, Supporting Information). Similar to dcHSA-PEG (**1**), DOX-dcHSA-PEG (**3**)

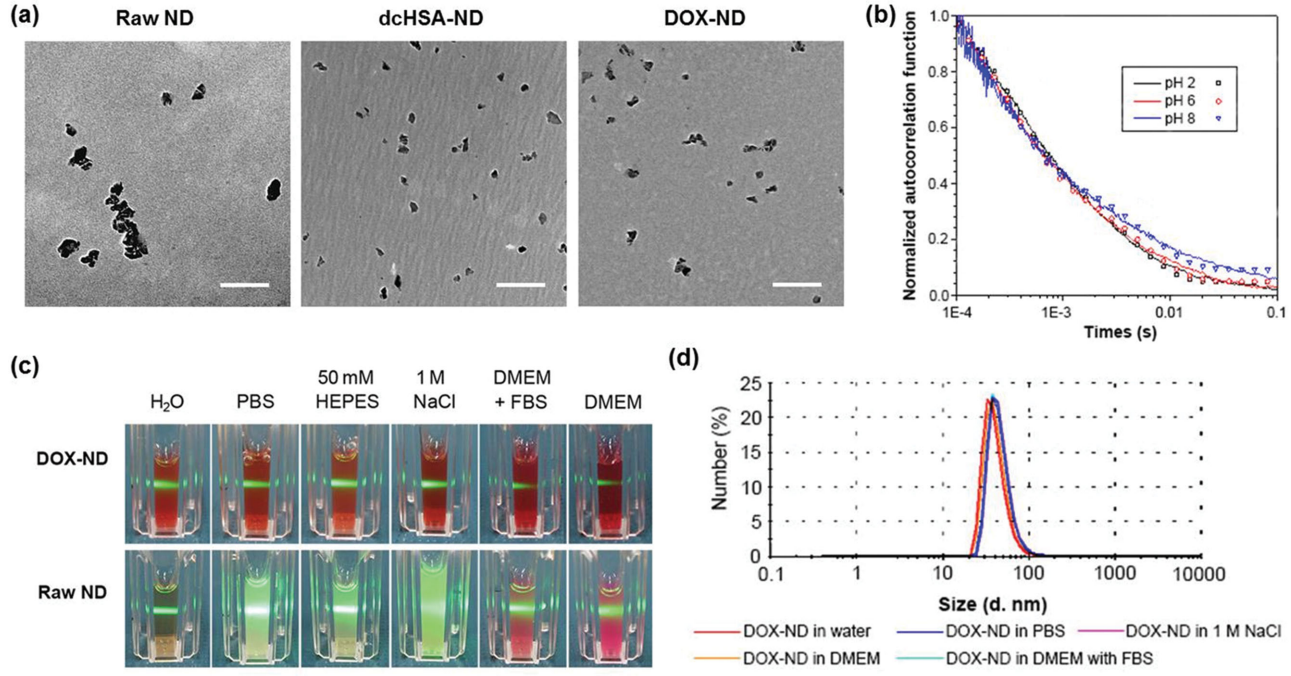

Figure 2. Characterization of dcHSA-NDs **2** and DOX-NDs **4**. a) TEM images show the raw NDs without coating as inhomogeneous aggregations, while dcHSA-NDs **2** and DOX-NDs **4** are mainly observed as single ND particles. Scale bar: 200 nm. b) FCS autocorrelation curves of dcHSA-NDs between pH 2.0 and pH 8.0. c) Photographs of 1 mg mL^{-1} DOX-NDs and raw NDs suspended in different physiologically relevant solutions, respectively. The green laser beam does not scatter in DOX-ND samples and in ND aqueous solution indicating no visible particle aggregation in solution. In contrast, the laser beam strongly scatters in raw ND samples suspended in PBS, 50×10^{-3} M HEPES pH 7.5, 1 M NaCl, and DMEM medium with/without 20% FBS due to aggregate formation. d) DLS chromatogram of DOX-NDs in water, PBS, HEPES buffer, 1 M NaCl, and DMEM with/without 20% FBS.

remained highly positively charged (zeta potential = 28.4 ± 0.6 mV) suitable for ND coating.

2.1.3. Biofunctionalization of NDs/FNDs

Coating of the NDs with biopolymers dcHSA-PEG (**1**) and DOX-dcHSA-PEG (**3**) was accomplished by slowly adding low concentrations of the NDs (0.1 mg mL^{-1}) into the diluted solution ($<1 \times 10^{-6}$ M) of the respective biopolymer under vigorous stirring. After coating, the respective NDs (dcHSA-ND **2** and DOX-ND **4**) were isolated, purified by centrifugation and washed with water to remove any unbound polymers (Figure 1). Drug loading of DOX-NDs was determined and about 5 wt% DOX was successfully loaded to the NDs by this method (see the Supporting Information for details).

The zeta potential of biopolymer-coated NDs changed from the negative to the positive (**2** = 18.4 ± 1.4 mV, **4** = 29.1 ± 1.1 mV, Figure S11, Supporting Information) and the hydrodynamic diameters in water increased to 69.3 ± 0.3 nm (**2**, PDI = 0.09) and 82.7 ± 0.6 nm (**4**, PDI = 0.21) (Figure S12, Supporting Information). Fourier transform infrared spectroscopy of dcHSA-NDs revealed the characteristic amide I and amide II absorbances at 1653 and 1541 cm^{-1}, and a significantly increased signal at 1101 cm^{-1}, attributed to C–N stretching of primary amines and C–O–C stretching of polyethylene glycol chains (Figure S13, Supporting Information). X-ray photoelectron spectroscopy of dcHSA-NDs indicated S2p3/2 BE of 162.6 eV, attributed to S (–II) sulfur of the polypeptide backbone and S2p3/2 BE of 167.7 eV relating to S (+VI) from sulfate (SO_4^{2-}) anions due to the sulfuric acid treatment used to remove graphitic carbon during ND preparation (Figure S14, Supporting Information).

Before coating, NDs displayed significant aggregate formation as shown by transmission electron microscopy (TEM, **Figure 2**a). In contrast, dcHSA-NDs (**2**) were only observed as single ND particles (Figure 2a and Figure S9, Supporting Information). Most ND formulations aggregate and precipitate in buffers with high salt concentrations (Table S2 and Figure S15, Supporting Information). However, dcHSA-NDs (**2**) were highly stable even in 1 M NaCl solution (Figure S15, Supporting Information) over long time periods (>1 month) and also within a broad pH range. Comparable diffusion times of the fluorescent dcHSA-NDs (**2**) were observed from pH 2.0 to pH 8.0 via fluorescence correlation spectroscopy (FCS), with minor variations of the hydrodynamic diameters around 90 nm demonstrating high colloidal stability even under acidic and basic conditions (Figure 2b). Since different body fluids exhibit substantial pH variations, stability within a broad pH range is a prerequisite for many biomedical applications.

Even though high quantities of aromatic drug DOX were attached to DOX-NDs (**4**), the colloidal stability still remained excellent under all tested conditions. On TEM, only single ND particles were found without any agglomeration (Figure 2a; Figures S9 and S10, Supporting Information). DOX-NDs (**4**) also displayed outstanding stability in different physiologically relevant buffer systems including phosphate buffered saline (PBS), 4-(2-hydroxyethyl)-1-piperazineethanesulfonic acid (HEPES)

buffer, Dulbecco's modified Eagle's medium (DMEM) cell culture medium with and without fetal bovine serum (FBS) supplementation (Figure 2c) and even at high salt concentrations (1 M NaCl), which has not been reported for any other ND coating yet (Figure 2c and Table S2, Supporting Information).[24] DLS measurements also indicated no changes of the size distribution of DOX-NDs under all tested conditions (Figure 2d; Figure S16 and Table S1, Supporting Information). Noteworthy, despite the high affinity of both ND and DOX for plasma proteins, DOX-ND complexes displayed high colloidal stability without changes in size distribution even in cell culture medium containing plasma proteins. We believe that this remarkable colloidal stability is due to the double shell architecture with the inner polypeptide shell attached to the ND surface containing the covalently loaded DOX molecules as well as the outer hydrophilic PEG shell protecting both the ND core and DOX molecules by supplying an extended hydration shell.[25]

2.2. NDs/FNDs as Powerful Probes to Directly Monitor Intracellular Drug-Particle Pathways

2.2.1. Intracellular Characterization and Monitoring of DOX Release

Both dcHSA-NDs and DOX-NDs were tested regarding their cellular toxicity and membrane uptake. dcHSA-NDs represent the "drug delivery platform" before drug modification and therefore low cellular toxicity of the "bare" nanotransporter would be highly desirable. Up to now, many positively charged nanoparticles have been studied and in most cases, efficient trafficking into mammalian cells was reported[26] accompanied with significant cytotoxicity due to their disruption of the cellular membrane.[27] The cellular uptake of dcHSA-NDs (**2**) was tested in the human lung adenocarcinoma cell line A549, which represents a typical epithelial cancer cell line used for drug delivery studies. As depicted in **Figure 3**a, dcHSA-NDs (**2**) were efficiently transported into A549 cells, where they homogenously distributed inside endosomal vesicles. They display remarkably low cellular toxicity even at very high concentrations up to 3 mg mL^{-1} in five tested cell lines (four adherent cell lines—A549, Hela, MDA-MB-321, PC-3 and one suspension cell line CCRF-CEM), which is a significant improvement compared to other reported platforms (Figure 3b and Table S2, Supporting Information including references). In contrast, noncoated NDs were not taken up by cells due to the negatively charged surface but some aggregate formation occurred at the cellular membrane (Figure 3a). Moreover, an in vitro test with J774 macrophages showed that dcHSA-NDs (up to 80 μg mL^{-1}) did not activate macrophages when incubated for 72 h (Figure S18, Supporting Information). To that effect, dcHSA-NDs are not expected to trigger inflammatory reactions upon in vivo applications.

DOX-NDs (**4**) contain multiple copies of therapeutic DOX molecules, which are covalently conjugated to the albumin polypeptide backbone via an acid labile hydrazone linker. The hydrazone linker was known to be stable at neutral and basic pH, e.g., as present in the blood stream but will be cleaved at acidic pH, e.g., below 5.0 as present in tumor tissue and within lysosomal compartments.[28,30a] This design was selected to reduce nonspecific drug release while circulating in the blood stream yet facilitating efficient drug release within the more acidic tumor cells and tissues. The acid triggered drug release was probed by incubating DOX-NDs (**4**) at pH 5.0 and pH 7.0. At different time points, the NDs were pelleted and DOX released into the bulk solution was quantified. Significant DOX release was observed at pH 5.0 within the first 12 h and at maximum 60% of total DOX was released from the NDs (**Figure 4**a) after 48 h. In contrast, less than 15% of DOX was released at pH 7.0 after 48 h

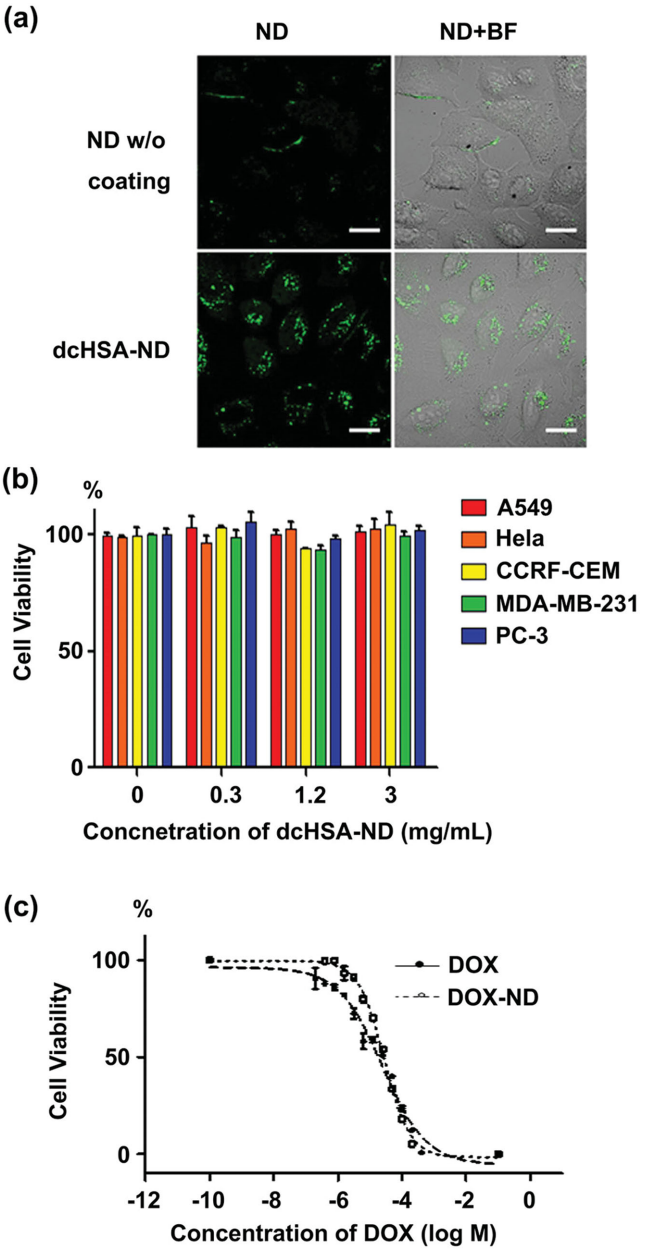

Figure 3. Cell uptake and cytotoxicity studies of dcHSA-NDs and DOX-NDs. a) Confocal imaging of fluorescent dcHSA-NDs inside A549 cells after 24 h incubation in comparison to raw fluorescent NDs without coating as negative control (ND concentration: 33 μg mL^{-1}) (BF = bright field). Scale bar: 20 μm. b) Cell viability of dcHSA-NDs with different cell lines after 24 h incubation. c) Cytotoxicity assay of free DOX and DOX-NDs **4** with A549 cells after 24 h incubation.

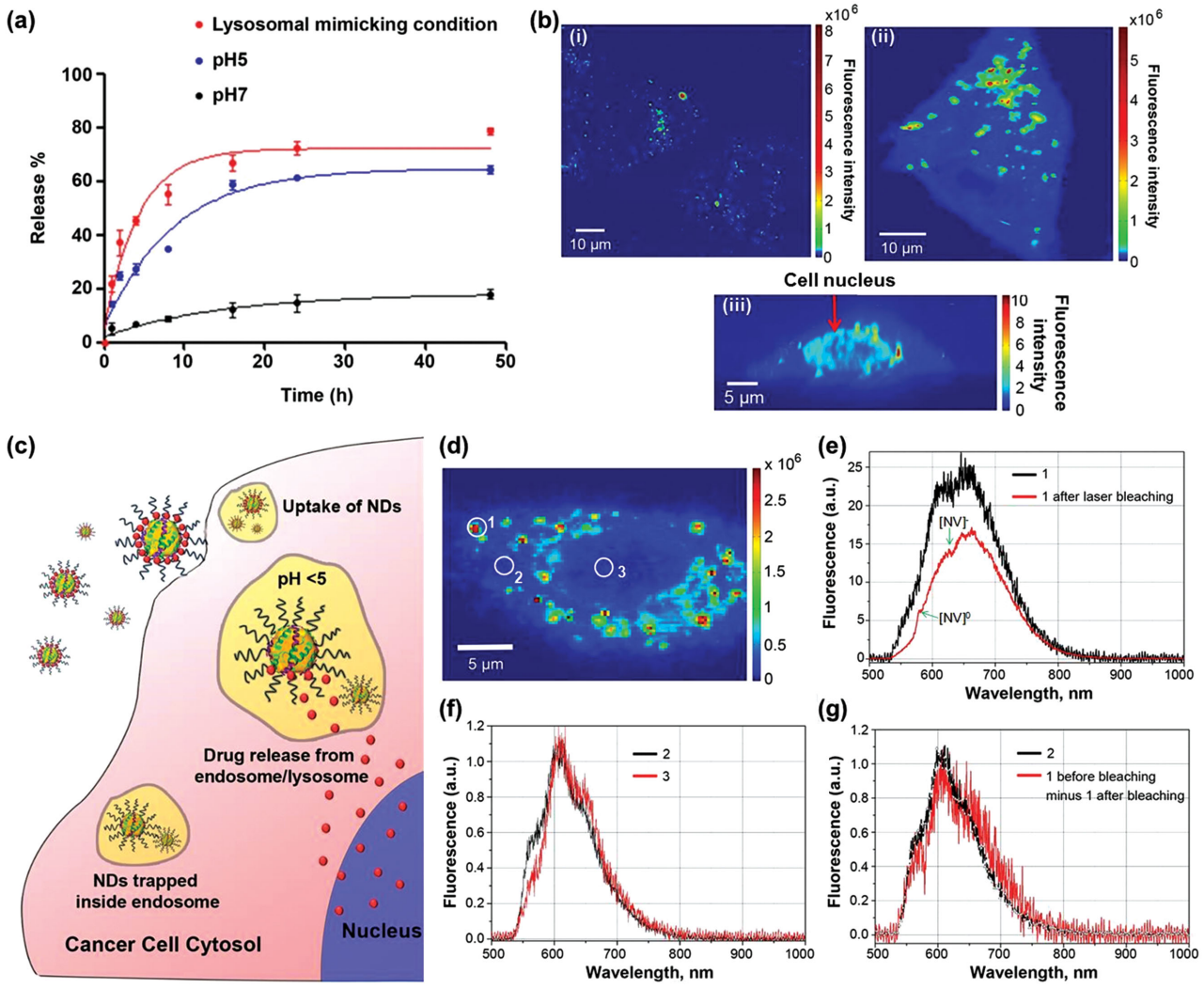

Figure 4. Acid-triggered DOX release from NDs tested in different buffers and in living cells. a) DOX release from DOX-NDs measured in pH 5.0 and pH 7.0 sodium phosphate buffers as well as under lysosomal mimicking conditions (0.5 U mL^{-1} cathepsin B, 24.6×10^{-3} M acetate, 1.1×10^{-3} M ethylenediaminetetracetic acid (EDTA), 0.33×10^{-3} M dithiothreitol (DTT), pH 5.0). b) Confocal microscope imaging of i) fluorescent dcHSA-NDs **2** and ii) fluorescent DOX-NDs **4** (11 μg mL^{-1} for both samples) added to A549 cells for 24 h. The z-axis scanning is shown in panel (iii). c) Illustration of zhe cell uptake and drug release process of DOX-ND. d) Fluorescence spectra inside living cells. A549 cells were treated with 55 μg mL^{-1} of fluorescent DOX-NDs for 24 h. Fluorescence spectra were recorded at the positions highlighted by white circles using a 504 nm excitation laser and a 532 nm long path filter in front of the detector. e) Representative emission spectra inside cellular vesicles (black line), e.g., circle 1, corresponds to the overlapping spectra of DOX and N-V centers. The emission spectrum after laser bleaching of the DOX emission (red line) yielding a typical emission spectrum of N-V centers with assignable peaks from $[N\text{-}V]^0$ and $[N\text{-}V]^-$. f) The representative emission spectra within the cytosol (black line), e.g., circle 2, and inside the nucleus (red line), e.g., circle 3, both revealing typical DOX spectra. g) The emission spectrum subtracted from the spectrum inside cellular vesicles before and after bleaching (500 μW for 5 min) yields the typical DOX emission similar to the spectra recorded in cytosol circle 2.

(Figure 4a). To better mimic the drug release kinetics within lysosomes, DOX-NDs (**4**) were also incubated under in vitro conditions mimicking the lysosomal environment at pH 5.0 in the presence of the lysosomal enzyme cathepsin B at relevant concentrations (see the Experimental Section for details). Under these conditions, DOX release was further boosted to a maximum level of about 70% after 24 h (Figure 4a) due to the degradation of HSA backbone by cathepsin B.[21] Noteworthy, even under such acidic and proteolytic conditions, no ND aggregation was observed.

Thereafter, DOX release from NDs was monitored by confocal microscopy imaging (Figure 4b). When cells were treated with fluorescent dcHSA-ND (**2**), no emission was detected within the cytosol, indicating that NDs were mainly trapped in endosomal vesicles. However, when cells were incubated with fluorescent DOX-ND (**4**), significant fluorescence originating from DOX molecules was observed within the cytosol as well as in the cell nucleus (Figure 4b). To confirm the origin of the fluorescent component within different cellular compartments, the fluorescence spectra were recorded inside cell vesicles, the cytosol, and the nucleus. As shown in Figure 4e, the emission spectrum within cell vesicles consists of overlapping emission spectra of DOX and the N-V centers of NDs. After applying strong laser light (500 μW for 5 min), the emission of DOX

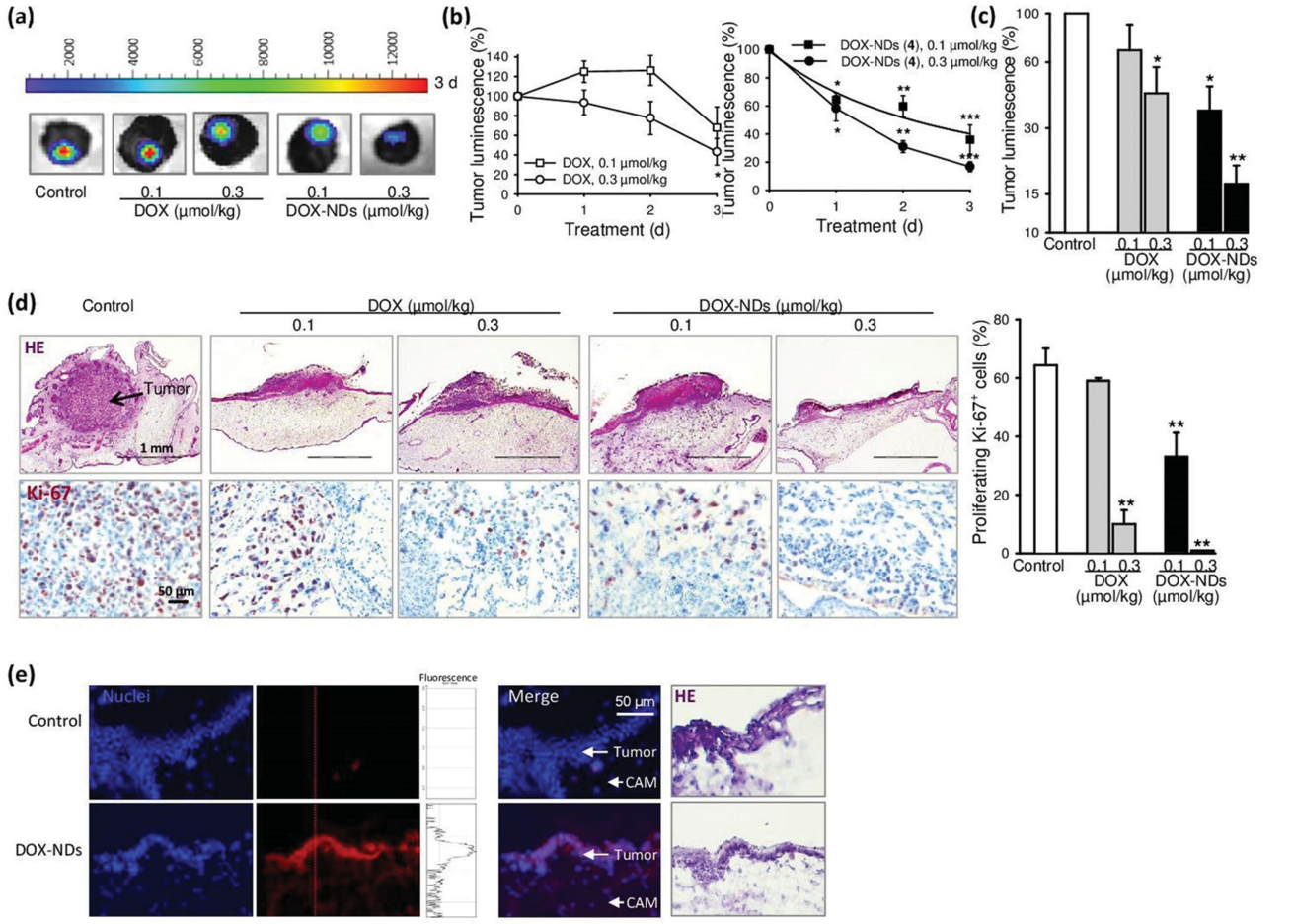

Figure 5. Antitumor effect of DOX-NDs on breast cancer xenografts in the CAM model. a) DOX-NDs decrease the viability of human cancer xenografts in vivo. Breast cancer cells (0.5×10^6 MDA-MB-231) stably expressing firefly luciferase were grafted onto the chorioallantoic membrane (CAM) of the chick embryo. One day later, xenografts were topically treated with 20 µL of either DOX or the equivalent concentrations of DOX-NDs in 0.9% NaCl. Tumor luminescence was analyzed by IVIS in vivo imaging 1–3 d after treatment and 10 min after addition of D-luciferin with integration time 1 s. Representative tumors are shown. b) Decrease in tumor growth was monitored by expression of luciferase by MDA-MB-231 cancer xenografts. The data are mean ± SEM (standard error of the mean) of $n = 4$–5. c) Tumor xenograft growth after 3 d treatment as analyzed by luminescence imaging. d) Immunohistochemical analysis of breast cancer xenografts. HE, hematoxilin and eosin staining of whole xenografts grown on CAM; original magnification 50×; Ki-67 antigen staining of tumor xenografts, brown-red nuclei are indicative of proliferating cells, original magnification, 200×. $^*P < 0.05$, $^{**}P < 0.01$, Newman–Keuls multigroup comparison. e) Analysis of selective DOX-NDs accumulation in tumor xenografts by using fluorescence microscopy. Frozen sections of tumor xenografts were stained with 4′,6-diamidino-2-phenylindole (DAPI, nuclei, blue) and fluorescent DOX-NDs were visualized with a red filter set (emission wavelength 610 nm). Graphs right to DOX-NDs images demonstrate changes in fluorescence intensity across the image (red line). The corresponding successive cuts were stained with HE to reveal morphology. Original magnifications, 200×.

was bleached and only the emission originating from the NDs was recorded and assigned clearly, due to the presence of the emission peaks of $[N\text{-}V]^0$ and $[N\text{-}V]^-$. By subtracting these two spectra before and after laser bleaching, a typical emission spectrum of DOX was calculated (Figure 4g, red line) substantiating the presence of DOX emission inside cell vesicles before laser bleaching. Interestingly, only DOX emission was found in the cytosol and within the nucleus without contribution of the N-V center emission (Figure 4f). These experiments clearly prove the release of DOX from the ND carriers and DOX escape from the endosomes and lysosomes. In contrast, NDs remained inside cellular vesicles and did not traffic into the cytosol. This behavior is most likely one of the reasons for the low cellular toxicity of the coated NDs since interfering with cellular processes is less likely to occur. Trapping NDs inside lysosomes is advantageous since excretion from the cells occurs more efficiently compared to nanoparticles located in the cytoplasm.[29] Therefore, distinct cellular compartmentalization of NDs and their cargo molecules could be beneficial to optimize the therapeutic efficacy of DOX and to promote ND excretion after delivery, which would be favorable for achieving translational drug delivery systems.

The cytotoxicity of DOX-NDs was tested in A549 cells after 24 h to allow sufficient time for DOX release. ND-bound DOX induces toxicity similar to free DOX (half maximal inhibitory concentration (IC_{50}) of DOX-ND = 27×10^{-6} M and IC_{50} of free DOX = 24×10^{-6} M, Figure 3c) indicating very efficient DOX release from the ND drug delivery system. This result is

remarkable because often, considerably reduced cytotoxicity of nanotransporter-complexed DOX compared to free DOX has been reported, which has been attributed to slow and inefficient drug release from the carrier.[30]

2.3. DOX-Loaded NDs/FNDs Exhibit Pronounced Antitumor Efficacy in a Human Breast Cancer Xenograft Model

Breast cancer is the most common malignancy in women, which is frequently further complicated by metastases to distant organs. In view of the disparity of therapeutic efficacy between primary tumors and advanced metastases, treatment of breast cancer remains a challenging task.[31] The successful identification and validation of novel, more effective anticancer drugs and delivery systems depends largely on the availability of suitable xenograft tumor models allowing cancer cells to grow in an appropriate microenvironment.[32]

We have previously established a special model, the chick chorioallantoic membrane model (CAM), that has been developed and validated to study anticancer compounds.[33] In this model, human cancer cells are xenotransplanted onto the chorioallantoic membrane of fertilized chicken eggs. The CAM model offers many unique advantages: It contributes to animal welfare by saving mammalian laboratory animals and above all, the growth of the xenotransplanted cancer cells in the tissue environment of the chorioallantoic membrane provides an efficient in vivo xenograft model even including the induction of neoangiogenesis. We have shown that data obtained in this model correlate well with in vivo experiments in mice[33,34] rendering it well suited for screening purposes before xenotransplantations in murine models should be conducted.

DOX-NDs exhibited significant antitumor efficacy in our in vivo model of MDA-MB-231 triple negative human breast cancer xenografts. Triple-negative breast cancer cells lack estrogen and progesterone receptor expression as well as human epidermal growth factor receptor 2 (HER2) amplification. This type of cancer constitutes 10%–20% of all breast cancers, where treatment has been particularly challenging.[35] DOX-NDs time- and dose-dependently inhibited bioluminescence of transgenic human breast cancer tumors stably expressing luciferase indicating inhibition of tumor growth. Strikingly, the antitumor effect of DOX-NDs was superior to that of free DOX[36] (**Figure 5**a–c). The inhibition of tumor growth by DOX-NDs was likewise confirmed by immunohistochemical analysis (Figure 2d). DOX-NDs and free DOX both reduced the cancer cell proliferation in a dose-dependent manner, as evidenced by the reduced number of nuclei expressing the proliferation antigen Ki-67 (Figure 5d). Yet, in comparison to free DOX, DOX-NDs exhibited in vivo faster antitumor kinetics (Figure 5d,b) and significantly more antitumor activity in comparison to free DOX. This is most likely due to the high local concentrations of DOX yielding from the enhanced permeability and retention effect that is possibly combined with a decreased efflux of bound DOX by drug transporters. To further prove this, frozen sections of tumor xenografts were analyzed and DOX fluorescence was only observed in tumor xenografts but not in the healthy tissue around the tumor (Figure 5e) indicating the successful accumulation of DOX in tumor tissue.

3. Conclusion

In conclusion, we have created a multifunctional and versatile biopolymer platform by chemical reprogramming human serum albumin, which is ideally suited to functionalize FNDs. The biopolymer modified FNDs displayed excellent colloidal stability under all physiological conditions tested, and also showed efficient cell uptake and excellent biocompatibility. Premodification of the biopolymers addressing the large number of reactive amino acid residues allows access to customized FNDs providing a large array of desired functionalities at their surface, which is particularly attractive for developing multifuctional FNDs for biomedical applications. As an example, a defined number of the anticancer drug molecule DOX were attached to the biopolymer before coating. The subsequently prepared DOX loaded FNDs featured unique bioimaging potential as well as potent anticancer efficiency. Even after loading with aromatic DOX molecules, the FNDs still remained highly stable in physiological media and high salt concentration solutions without forming aggregations, which is significant in comparison to previously reported systems. High colloidal stability is of great significance for in vivo applications to achieve sufficient stability and circulation in the blood stream since uncontrolled aggregation of nanoparticles is connected with unexpected cellular toxicities and therefore, stability of nanomaterials is a critical concern for their clinical development.[37] High numbers of DOX molecules were linked to FNDs by an acid-cleavable linker and were efficiently transported and released inside cancer cells: The intracellular distribution of NDs and DOX was resolved in live cells by recording the fluorescence spectra of NDs and DOX in different cellular compartments. Significant amounts of DOX were released from ND carriers and distributed inside the cytoplasm and the nucleus, whereas the ND carriers remained entrapped inside endosomal vesicles. Studies with cancer cells in vitro as well as with chicken embryo models underlined the efficient antitumor effect of DOX-NDs.

Due to their biocompatibility and unique magnetooptical properties, we envision that functionalized FNDs will emerge as safe "metal-free" nanotransporters offering many valuable features compared to other known nanoparticle emitters such as semiconductor quantum dots or gold nanoparticles. The versatile biopolymer coating strategy reported herein will greatly accelerate the availability of customized NDs with reliable and reproducible features to exploit their great potential in single molecule bioimaging, in vivo biosensing and high resolution quantum optics. Together with the promising application of NDs as drug delivery carriers, this strategy could be particularly attractive for developing multimodal NDs combining therapy and imaging potential in one particle for the emerging concept of "theranostics."

4. Experimental Section

Preparation of dcHSA-NDs ***2*** *and DOX-NDs* ***4***: dcHSA-PEG, DOX-dcHSA-PEG, and NDs were prepared according to reported protocols[17,21,38] and explained in the Supporting Information. NDs (10 mg) were dispersed in boric acid buffer (100 mL, 20×10^{-3} M, pH = 8.4) and ultrasonicated for 1 h. dcHSA-PEG (34.66 mg, 0.33 mmol) (in case of preparing DOX-NDs **4**, we used DOX-dcHSA-PEG (40 mg, 0.33 mmol)) was dissolved in boric acid buffer (400 mL, 20×10^{-3} M, pH = 8.4) and

stirred at room temperature for 30 min. Then, ND solution was dropwise added to dcHSA-PEG/DOX-dcHSA-PEG solution for 1 h and stirred at room temperature overnight. Thereafter, the reaction mixture was concentrated by ultrafiltration to 5 mL, then the uncoated dcHSA-PEG was washed out by centrifugation of dcHSA-NDs **2** (or DOX-NDs **4**) (17 000*g*, 30 min) and resuspended in water by ultrasonication (30 min) more than eight times. Then the dcHSA-NDs/DOX-NDs were resupended in 5 mL water (dcHSA-NDs **2** obtained 1.52 mg mL^{-1}, yield 45%; DOX-NDs **4** obtained 1.7 mg mL^{-1}, yield 40%).

Measuring Kinetics of Drug Release: The DOX release profile was determined in pH 5.0 sodium phosphate buffer (20×10^{-3} M) and pH 7.4 sodium phosphate buffer (20×10^{-3} M) as well as under an in vitro condition mimicking the lysosomal environment. The lysosomal mimicking condition was prepared by adding cathepsin B to the activation buffer (30×10^{-3} M DTT, 15×10^{-3} M EDTA) to a final concentration of 1.6 U mL^{-1} cathepsin B, 20×10^{-3} M DTT, 10×10^{-3} M EDTA and preincubated at 37 °C for 15 min. DOX-NDs **4** (0.58 mg, contains 15 nmol of DOX) were suspended in 50 µL of pH 5.0 buffer, pH 7.4 buffer, and preactivated cathepsin B solution, respectively. The reaction solution was incubated at 37 °C. Aliquots were removed at desired time points and pelleted by centrifugation (17 000*g*, 30 min). The amount of DOX release in supernatant was determined by measuring the DOX absorbance at 488 nm.

Confocal Microscopy Imaging and Fluorescence Spectrum Measurement in Live Cells: In order to prove the DOX release from NDs in living cells, free DOX, the fluorescent DOX-NDs **4**, and dcHSA-NDs **2** were investigated on an in-house built high resolution confocal microscope equipped with a camera from Excelitas Technologies (SPCM-AQRH-14) and spectrometer from Princeton Instruments. The A549 cells were treated with DOX (0.55 µg mL^{-1}, 1×10^{-6} M), fluorescent dcHSA-NDs **2** (11 µg mL^{-1}), and fluorescent DOX-NDs **4** (11 µg mL^{-1}, containing DOX at a concentration of 0.55 µg mL^{-1}, 1×10^{-6} M) for 24 h and washed three times with phosphate buffer saline before imaging. Confocal microscopy images were taken with 532 nm laser excitation and 560 nm filter. To prove that the fluorescence inside the cells originates from N-V centers and DOX, the fluorescence spectra were taken. For this experiment, A549 cells were treated with higher concentrations of DOX (5×10^{-6} M) and DOX-NDs (5.5 µg mL^{-1}, containing DOX at a concentration of 5×10^{-6} M) for 24 h. Since the emission spectrum of DOX is slightly blue shifted with respect to N-V emission, excitation was at 504 nm and cutoff of the long pass filter in front of the spectrometer was set at 532 nm. The obtained images were processed with MatLab.

Xenografts Tumor Model: The MDA-MB-231 breast cancer cell line stably expressing firefly luciferase was obtained from Cell Biolabs (San Diego, CA). For the in vivo experiments, MDA-MB-231 xenografts (0.5×10^6 cells) were grafted in medium/Matrigel (1:1, v/v) onto the chorioallantoic membrane (CAM) of chick eggs on day 8 after fertilization.[33,39] The next day, the xenografts were topically treated for three consecutive days with 20 µL of either free DOX or DOX-NDs to yield doses of 0.1 and 0.3 µmol kg^{-1}. Tumor luminescence was analyzed on days 1–3 after initiation of the treatment and 15 min after addition of D-luciferin (0.75 mg mL^{-1}, 10 µL) with an integration time of 1 s using an IVIS In Vivo Imaging System (IVIS, Perkin Elmer, Waltham, MA). On day 13 after fertilization, xenografts were collected, fixed, paraffin embedded, and histologically analyzed. Serial sections (5 µm) were stained for the human proliferation antigen Ki-67.[33,39]

Supporting Information

Supporting Information is available from the Wiley Online Library or from the author.

Acknowledgements

Y.W., A.E., and W.L. contributed equally to this work. This work was supported by the European Reseach Council Synergy Grant 319130-BioQ, Volkswagenstiftung and the Deutsche Forschungsgemeinschaft (SFB1149, project A04 of H.B. and T.W.). The authors thank Felicitas Genze for expert technical assistance and thank Robert Leiter and Haoyuan Qi for performing high resolution TEM experiment.

Received: July 2, 2015
Revised: August 8, 2015
Published online: October 8, 2015

[1] a) V. Vaijayanthimala, H. C. Chang, *Nanomedicine* **2008**, *4*, 47; b) V. N. Mochalin, O. Shenderova, D. Ho, Y. Gogotsi, *Nat. Nanotechnol.* **2012**, *7*, 11.
[2] a) G. Balasubramanian, I. Y. Chan, R. Kolesov, M. Al-Hmoud, J. Tisler, C. Shin, C. Kim, A. Wojcik, P. R. Hemmer, A. Krueger, T. Hanke, A. Leitenstorfer, R. Bratschitsch, F. Jelezko, J. Wrachtrup, *Nature* **2008**, *455*, 648; b) M. Börsch, R. Reuter, G. Balasubramanian, R. Erdmann, F. Jelezko, J. Wrachtrup, *Proc. SPIE* **2009**, *7183*, 71832N.
[3] H. Zhang, I. Aharonovich, D. R. Glenn, R. Schalek, A. P. Magyar, J. W. Lichtman, E. L. Hu, R. L. Walsworth, *Small* **2014**, *10*, 1908.
[4] a) P. Neumann, I. Jakobi, F. Dolde, C. Burk, R. Reuter, G. Waldherr, J. Honert, T. Wolf, A. Brunner, J. H. Shim, D. Suter, H. Sumiya, J. Isoya, J. Wrachtrup, *Nano Lett.* **2013**, *13*, 2738; b) T. Staudacher, F. Shi, S. Pezzagna, J. Meijer, J. Du, C. A. Meriles, F. Reinhard, J. Wrachtrup, *Science* **2013**, *339*, 561; c) A. Ermakova, G. Pramanik, J. M. Cai, G. Algara-Siller, U. Kaiser, T. Weil, Y. K. Tzeng, H. C. Chang, L. P. McGuinness, M. B. Plenio, B. Naydenov, F. Jelezko, *Nano Lett.* **2013**, *13*, 3305.
[5] a) J.-H. Liu, S.-T. Yang, X.-X. Chen, H. Wang, *Curr. Drug Metab.* **2012**, *13*, 1046; b) A. M. Schrand, H. Huang, C. Carlson, J. J. Schlager, E. Ōsawa, S. M. Hussain, L. Dai, *J. Phys. Chem. B* **2006**, *111*, 2.
[6] a) L. Kuang-Kai, C. Chia-Liang, C. Chia-Ching, I. C. Jui, *Nanotechnology* **2007**, *18*, 325102; b) A. M. Schrand, L. Dai, J. J. Schlager, S. M. Hussain, E. Osawa, *Diamond Relat. Mater.* **2007**, *16*, 2118; c) A. M. Schrand, H. Huang, C. Carlson, J. J. Schlager, E. Ōsawa, S. M. Hussain, L. Dai, *J. Phys. Chem. B* **2007**, *111*, 2.
[7] a) J. Li, Y. Zhu, W. Li, X. Zhang, Y. Peng, Q. Huang, *Biomaterials* **2010**, *31*, 8410; b) Y. Li, X. Zhou, D. Wang, B. Yang, P. Yang, *J. Mater. Chem.* **2011**, *21*, 16406; c) D. Wang, Y. Tong, Y. Li, Z. Tian, R. Cao, B. Yang, *Diamond Relat. Mater.* **2013**, *36*, 26; d) X.-Q. Zhang, R. Lam, X. Xu, E. K. Chow, H.-J. Kim, D. Ho, *Adv. Mater.* **2011**, *23*, 4770; e) L. Zhao, Y.-H. Xu, T. Akasaka, S. Abe, N. Komatsu, F. Watari, X. Chen, *Biomaterials* **2014**, *35*, 5393.
[8] R. A. Shimkunas, E. Robinson, R. Lam, S. Lu, X. Xu, X.-Q. Zhang, H. Huang, E. Osawa, D. Ho, *Biomaterials* **2009**, *30*, 5720.
[9] R. Martín, M. Álvaro, J. R. Herance, H. García, *ACS Nano* **2010**, *4*, 65.
[10] a) M. Chen, E. D. Pierstorff, R. Lam, S.-Y. Li, H. Huang, E. Osawa, D. Ho, *ACS Nano* **2009**, *3*, 2016; b) E. K. Chow, X.-Q. Zhang, M. Chen, R. Lam, E. Robinson, H. Huang, D. Schaffer, E. Osawa, A. Goga, D. Ho, *Sci. Transl. Med.* **2011**, *3*, 73ra21; c) H. Huang, E. Pierstorff, E. Osawa, D. Ho, *Nano Lett.* **2007**, *7*, 3305; d) L. Moore, V. Grobarova, H. Shen, H. B. Man, J. Micova, M. Ledvina, J. Stursa, M. Nesladek, A. Fiserova, D. Ho, *Nanoscale* **2014**, *6*, 11712.
[11] a) K. K. Liu, W. W. Zheng, C. C. Wang, Y. C. Chiu, C. L. Cheng, Y. S. Lo, C. Chen, J. I. Chao, *Nanotechnology* **2010**, *21*, 315106; b) L. Zhao, Y.-H. Xu, H. Qin, S. Abe, T. Akasaka, T. Chano, F. Watari, T. Kimura, N. Komatsu, X. Chen, *Adv. Funct. Mater.* **2014**, *24*, 5348.
[12] a) T. B. Toh, D. K. Lee, W. Hou, L. N. Abdullah, J. Nguyen, D. Ho, E. K. Chow, *Mol. Pharm.* **2014**, *11*, 2683; b) J. Xiao, X. Duan, Q. Yin, Z. Zhang, H. Yu, Y. Li, *Biomaterials* **2013**, *34*, 9648.

[13] R. Kaur, I. Badea, *Int. J. Nanomed.* **2013**, *8*, 203.
[14] a) Z. Liu, X. J. Liang, *Theranostics* **2012**, *2*, 235; b) Y. Zhu, J. Li, W. Li, Y. Zhang, X. Yang, N. Chen, Y. Sun, Y. Zhao, C. Fan, Q. Huang, *Theranostics* **2012**, *2*, 302.
[15] A. Krueger, D. Lang, *Adv. Funct. Mater.* **2012**, *22*, 890.
[16] a) L. Zhao, Y.-H. Xu, H. Qin, S. Abe, T. Akasaka, T. Chano, F. Watari, T. Kimura, N. Komatsu, X. Chen, *Adv. Funct. Mater.* **2014**, *24*, 5348; b) D. Wang, Y. Tong, Y. Li, Z. Tian, R. Cao, B. Yang, *Diamond Relat. Mater.* **2013**, *36*, 26; c) L. Zhao, T. Takimoto, M. Ito, N. Kitagawa, T. Kimura, N. Komatsu, *Angew. Chem. Int. Ed.* **2011**, *50*, 1388; d) X.-Q. Zhang, M. Chen, R. Lam, X. Xu, E. Osawa, D. Ho, *ACS Nano* **2009**, *3*, 2609; e) A. Bumb, S. K. Sarkar, N. Billington, M. W. Brechbiel, K. C. Neuman, *J. Am. Chem. Soc.* **2013**, *135*, 7815; f) I. Rehor, J. Slegerova, J. Kucka, V. Proks, V. Petrakova, M.-P. Adam, F. Treussart, S. Turner, S. Bals, P. Sacha, M. Ledvina, A. M. Wen, N. F. Steinmetz, P. Cigler, *Small* **2014**, *10*, 1106.
[17] Y. Wu, G. Pramanik, K. Eisele, T. Weil, *Biomacromolecules* **2012**, *13*, 1890.
[18] a) M. Chen, E. D. Pierstorff, R. Lam, S. Y. Li, H. Huang, E. Osawa, D. Ho, *ACS Nano* **2009**, *3*, 2016; b) K. K. Liu, W. W. Zheng, C. C. Wang, Y. C. Chiu, C. L. Cheng, Y. S. Lo, C. Chen, J. I. Chao, *Nanotechnology* **2010**, *21*, 315106.
[19] J. W. Lee, S. Lee, S. Jang, K. Y. Han, Y. Kim, J. Hyun, S. K. Kim, Y. Lee, *Mol. BioSyst.* **2013**, *9*, 1004.
[20] S. L. Kuan, Y. Wu, T. Weil, *Macromol. Rapid Commun.* **2013**, *34*, 380.
[21] Y. Wu, S. Ihme, M. Feuring-Buske, S. L. Kuan, K. Eisele, M. Lamla, Y. Wang, C. Buske, T. Weil, *Adv. Healthcare Mater.* **2013**, *2*, 884.
[22] M. E. Price, R. M. Cornelius, J. L. Brash, *Biochim. Biophys. Acta, Biomembr.* **2001**, *1512*, 191.
[23] a) D. L. Hershman, R. B. McBride, A. Eisenberger, W. Y. Tsai, V. R. Grann, J. S. Jacobson, *J. Clin. Oncol.* **2008**, *26*, 3159; b) C. J. Schmitt, S. Dietrich, A. D. Ho, M. Witzens-Harig, *Ann. Hematol.* **2012**, *91*, 391.
[24] H. Huang, E. Pierstorff, E. Osawa, D. Ho, *Nano Lett.* **2007**, *7*, 3305.
[25] S.-D. Li, L. Huang, *J. Controlled Release* **2010**, *145*, 178.
[26] O. Harush-Frenkel, N. Debotton, S. Benita, Y. Altschuler, *Biochem. Biophys. Res. Commun.* **2007**, *353*, 26.
[27] W. T. Godbey, K. K. Wu, A. G. Mikos, *J. Controlled Release* **1999**, *60*, 149.
[28] a) Y. Bae, S. Fukushima, A. Harada, K. Kataoka, *Angew. Chem. Int. Ed.* **2003**, *42*, 4640; b) H. S. Yoo, E. A. Lee, T. G. Park, *J. Controlled Release* **2002**, *82*, 17; c) J. Kalia, R. T. Raines, *Angew. Chem. Int. Ed.* **2008**, *47*, 7523.
[29] Z. Chu, Y. Huang, Q. Tao, Q. Li, *Nanoscale* **2011**, *3*, 3291.
[30] a) L. Zhao, Y. H. Xu, T. Akasaka, S. Abe, N. Komatsu, F. Watari, X. Chen, *Biomaterials* **2014**, *35*, 5393; b) K. Wang, X. Zhang, Y. Liu, C. Liu, B. Jiang, Y. Jiang, *Biomaterials* **2014**, *35*, 8735.
[31] J. Lu, P. S. Steeg, J. E. Price, S. Krishnamurthy, S. A. Mani, J. Reuben, M. Cristofanilli, G. Dontu, L. Bidaut, V. Valero, G. N. Hortobagyi, D. Yu, *Cancer Res.* **2009**, *69*, 4951.
[32] J. Killion, R. Radinsky, I. Fidler, *Cancer Metastasis Rev.* **1998**, *17*, 279.
[33] T. Syrovets, J. E. Gschwend, B. Büchele, Y. Laumonnier, W. Zugmaier, F. Genze, T. Simmet, *J. Biol. Chem.* **2005**, *280*, 6170.
[34] a) M. Vogler, H. Walczak, D. Stadel, T. L. Haas, F. Genze, M. Jovanovic, J. E. Gschwend, T. Simmet, K. M. Debatin, S. Fulda, *Cancer Res.* **2008**, *68*, 7956; b) A. C. Estrada, T. Syrovets, K. Pitterle, O. Lunov, B. Buchele, J. Schimana-Pfeifer, T. Schmidt, S. A. Morad, T. Simmet, *Mol. Pharmacol.* **2010**, *77*, 378.
[35] L. S. Adams, N. Kanaya, S. Phung, Z. Liu, S. Chen, *J. Nutr.* **2011**, *141*, 1805.
[36] D. E. Jenkins, Y. S. Hornig, Y. Oei, J. Dusich, T. Purchio, *Breast Cancer Res.* **2005**, *7*, R444.
[37] A. Radomski, P. Jurasz, D. Alonso-Escolano, M. Drews, M. Morandi, T. Malinski, M. W. Radomski, *Br. J. Pharmacol.* **2005**, *146*, 882.
[38] Y.-R. Chang, H.-Y. Lee, K. Chen, C.-C. Chang, D.-S. Tsai, C.-C. Fu, T.-S. Lim, Y.-K. Tzeng, C.-Y. Fang, C.-C. Han, H.-C. Chang, W. Fann, *Nat. Nanotechnol.* **2008**, *3*, 284.
[39] C. Loos, T. Syrovets, A. Musyanovych, V. Mailänder, K. Landfester, T. Simmet, *Biomaterials* **2014**, *35*, 1944.